DR. ALEXANDRE NORMANDEAU (Orcid ID: 0000-0001-7900-7763)

Article type : Original Manuscript

The influence of turbidity currents and contour currents on the distribution of deep-water sediment waves offshore eastern Canada

Alexandre Normandeau^{1*}, D. Calvin Campbell¹, Matthieu J.B. Cartigny²

¹ Geological Survey of Canada (Atlantic), Natural Resources Canada, Dartmouth, Nova

Scotia, Canada, B2Y 4A2

² Department of Earth Science and Geography, University of Durham, Durham, UK, DH1

3LY

*alexandre.normandeau@canada.ca

Associate Editor – Jaco Baas

Short Title – Bedforms in mixed turbidite–contourite systems

This article has been accepted for publication and undergone full peer review but has not been through the copyediting, typesetting, pagination and proofreading process, which may lead to differences between this version and the Version of Record. Please cite this article as doi: 10.1111/sed.12557

ABSTRACT

Sediment waves are commonly observed on the sea floor and often vary in morphology and geometry according to factors such as seabed slope, density and discharge of turbidity currents, and the presence of persistent contour currents. This paper documents the morphology, internal geometry and distribution of deep-water (4000 to 5000 m) bedforms observed on the sea floor offshore of Nova Scotia using high-resolution multibeam bathymetry data and seismic stratigraphy. The bedforms have wavelengths of >1 km but fundamentally vary in terms of morphology and internal stratigraphy and are distinguished into three main types. The first type, characterized by their long-wavelength crescentic shape, is interpreted as net-erosional cyclic steps. These cyclic steps were formed by turbidity currents flowing through canyons and overtopping and breaching levées. The second type, characterized by their linear shape and presence on levées, is interpreted as net-depositional cyclic steps. These upslope migrating bedforms are strongly aggradational, indicating high sediment deposition from turbidity currents. The third type, characterized by their obliqueness to canyons, is observed on an open slope and is interpreted as antidunes. These antidunes were formed by the deflection of the upper dilute, low-density parts of turbidity currents by contour currents. The modelling of the behaviour of these different types of turbidity currents reveals that fast-flowing flows form cyclic steps while their upper parts overspill and are entrained westward by contour currents. The interaction between turbidity currents and contour currents results in flow thickening and reduced sediment concentration, which leads to lower flow velocities. Lower velocities, in turn, allow the formation of antidunes instead of cyclic steps because the densiometric Froude number (Fr') decreases. Therefore, this study shows that both net-erosional and net-depositional cyclic steps are distributed along channels where turbidity currents prevail whereas antidunes form on open slopes, in a mixed turbidite/contourite system. This study provides insights into the influence

of turbidity currents versus contour currents on the morphology, geometry and distribution of bedforms in a mixed turbidite–contourite system.

Keywords: Antidunes, contour currents, cyclic steps, sediment waves, supercritical flows, turbidity currents

INTRODUCTION

Turbidity currents and contour currents transport large volumes of sediment to the sea floor and are important to the construction of continental margins (Faugères et al., 1999; Masson et al., 2002). Turbidity currents tend to construct large channel-levée complexes and submarine fans (Nakajima et al. 1998; Gonthier et al. 2003; Sylvester et al. 2011) whereas contour currents construct contourite drifts (Stow & Faugères, 2008; Rebesco et al., 2014). These two processes often operate simultaneously along a margin where contour currents remobilize sediment transported by turbidity currents (Faugères et al. 1999; Mulder et al. 2008; Gong et al. 2012, 2015; Campbell & Mosher 2016). However, the influence of this interaction on turbidity flow behaviour and bedform distribution and morphology has yet to be examined. Sediment waves are commonly observed on the sea floor and have wavelengths of tens to thousands of metres (Wynn & Stow, 2002; Symons et al., 2016); they form under a wide variety of currents, including contour currents (Rebesco et al., 2014; Campbell et al., 2016), internal waves (Ribó et al. 2016) and turbidity currents (Ercilla et al. 2002; Urgeles et al. 2009; Casalbore et al., 2014; Zhong et al. 2015; Normandeau et al. 2016). Sediment waves recognized in turbidite systems can be separated into three groups: scours, and small and large sediment waves (Symons et al., 2016). Most bedforms described in shallow (<500 m) and deep-water settings migrate upslope and can be classified as upper-flow regime

bedforms. The upslope migration indicates that they formed under Froude-supercritical turbidity currents (Fr' \geq 1). The ubiquity of upslope migrating bedforms in marine settings is explained by the ease of turbidity currents in reaching Fr' \geq 1 since submarine flows require low velocities to achieve such conditions (Kostic *et al.* 2010).

Upper-flow regime turbidity currents can form upslope migrating bedforms, such as cyclic steps and antidunes (Normark *et al.* 1980; Migeon *et al.* 2000; Fildani *et al.* 2006; Lamb *et al.* 2008; Covault *et al.* 2014) as well as lee-waves (Flood, 1988), which share similar characteristics to cyclic steps. Cyclic steps are here defined as long wavelength bedforms delimited at their downstream and upstream ends by hydraulic jumps. The current is supercritical on the lee sides (Fr' > 1) and subcritical on the stoss sides (Fr' < 1), immediately following the hydraulic jumps (Parker 1996). Conversely, antidunes are shorter wavelength bedforms where the undulations at the flow/water interface are in phase with those on the seabed (Kostic *et al.* 2010). Several studies are now reinterpreting previously documented antidunes as cyclic steps based on internal geometry and numerical modelling (Cartigny *et al.* 2011; Kostic 2011). The differentiation of these types of upper-flow regime sediment waves proves to be difficult without high-resolution multibeam and seismic reflection data or numerical modelling (Covault *et al.* 2017).

Offshore eastern Canada (Fig. 1), the widespread presence of sediment waves was recently recognized following mapping of the lower continental slope. This paper investigates the morphology, internal character and distribution of different types of sediment waves using newly acquired multibeam bathymetry and seismic reflection data. These analyses enable evaluation of the respective roles of contour and turbidity currents on sediment transport because both types of currents interact offshore The Gully Canyon (Campbell & Mosher 2016). Specifically, this study aims to: (i) differentiate the types of bedforms observed on the lower Scotian Slope; (ii) examine the controls over their distribution; and (iii) infer the flow

behaviour of turbidity currents travelling down the Scotian Slope. Ultimately, this study sheds new light on the role of contour versus turbidity current processes on the distribution, morphology and orientation of sediment waves.

REGIONAL SETTING

Physiographic setting

The Scotian margin consists of a 200 km wide continental shelf and an upper and lower slope located south of Nova Scotia (Fig. 1). The shelf contains transverse troughs and banks resulting from repeated glaciations over the region (Piper 2005). The shelf break, located at a depth of 80 to 130 m, leads to the highly incised Scotian Slope, which overlies a Mesozoic rifted passive continental margin comprised of Triassic salt, overlain by thick Mesozoic carbonates, sandstones and shales and Cenozoic progradational shales (Wade & MacLean 1990). The canyons formed during the late Pliocene, when climatic cooling and a low eustatic sea-level resulted in a direct connection between the coast and canyon heads, increasing glaciofluvial sediment delivery to the Scotian Slope (Piper & Normark, 1989). The canyons formed by repetitive turbidity current activity, triggered by glacial meltwaters.

Submarine canyons incise the continental shelf to a depth of 300 to 400 m. Thalweg gradients are typically 2° and increase locally to 15 to 25° within canyon heads. The canyons have steep (20°) sidewalls with numerous failure scarps on the ridges separating the canyons, highlighting the role of landslides in the downslope mobilization of sediment (Jenner *et al.* 2007). At *ca* 4000 m water depth, canyons and channels coalesce on the lower slope, forming long-running channels that extend onto the lower continental slope.

Contour currents

Bottom currents flow near the shelf break of the Scotian margin down to the lower slope (Fig. 1), and are mainly driven by Coriolis force. The main current, the North Atlantic Deep Western Boundary Current (DWBC), flows south-westward along the continental margin and consists of three distinct water masses (Pickart 1992): (i) the Upper Labrador Sea Water (ULSW), flowing at a depth of ca 700 m; (ii) the Classic Labrador Sea Water (CLSW) flows south-westward at ca 1500 m; and (iii) the Denmark Strait Overflow Water (DSOW) and Iceland-Scotland Overflow Water (ISOW) flow deeper and faster. This part of the DWBC directly affects the outer Gully region studied in this paper (Campbell & Mosher, 2016). Farther downslope, the eastward slope water filament stems from the deep Gulf Stream gyre. Bottom currents constructed contourite drifts along the Scotian Slope and were particularly active during the Neogene (Campbell & Mosher, 2016). The contourite drifts are characterized by large sediment waves forming stacked, aggrading sequences. Near the study area, the large buried Gully drift forms a narrow sedimentary ridge perpendicular to the orientation of the margin (Fig. 1). It is interpreted as a contouritic levée that is linked to the adjacent channel system through the interaction of turbidity currents and bottom currents (Campbell & Mosher 2016).

METHODS

Deep-water high-resolution bathymetric data were collected in 2012 on board the *R/V Atlantis* using a hull mounted 12 kHz Kongsberg EM122 multibeam sonar (Kongsberg Maritime AS, Kongsberg, Norway) coupled with a XYSEA PHINS integrated motion sensor. Positioning was provided by a satellite corrected CNav GPS (Oceaneering, Houston, TX, USA) CNav GPS and real-time sound speed was acquired using a Seabird TSG velocity

sounder (SeaBird Exploration AS, Oslo, Norway). Expendable bathythermograph sound speed profilers were recalculated using the 2009 World Ocean Atlas database salinity profiles and imported in real time to the navigation and acquisition software (SIS). The EM122 has a 64° swath angle and 865 beams. The raw data were imported into Caris HIPS and SIPSTM and gridded at 60 m resolution. Backscatter intensity information was processed using Caris HIPS and SIPS Geocoder engine and gridded at 40 m.

During the *R/V Atlantis* cruise, 3.5 kHz Knudsen sub-bottom profiler data (Knudsen Engineering Limited, Perth, Ontario, Canada) were acquired along the same lines as the multibeam data, i.e. mostly parallel to the depth contour. In 2016, a marine geology expedition on CCGS Hudson (Campbell & Normandeau, 2018) acquired seismic reflection data using a Huntec deep tow system with a sparker source. The acoustic output was centred on *ca* 1.5 kHz, with a 0.5 to 2.5 kHz bandwidth. Single channel streamer and 3.4 L Generator-Injector (GI) gun data were also collected in 2016 to image deeper reflections. The sub-bottom data were then imported and analyzed in The Kingdom Suite[©] software.

Piston core 2016011-PH1-02 (hereafter referred as 'core 2') was collected in 2016 on the CCGS Hudson. It was processed through a medical Computed Tomography (CT) core scanner, then opened and described. CT-numbers were extracted and mainly reflect changes in density (Fortin et al., 2013). Accelerator mass spectrometry (AMS) 14 C dating was performed on planktonic foraminifera at the base of core 2. Radiocarbon ages were calibrated using Calib 7.0 (Stuiver & Reimer, 1993) with the Reimer et al. (2013) Marine 13 dataset (Table 1), which applies a 400 yr ($\Delta R - 0$ yr) reservoir correction.

RESULTS

Morphology of the continental slope

The Scotian Slope consists mostly of submarine canyons that merge downslope into channels (Mosher *et al.* 2004). Most canyon heads are slope-confined although the Gully, Shortland and Haldimand canyons indent the shelf edge in the study area and form a dendritic drainage pattern, with gullies merging into larger canyons.

West of Laurentian Fan (Fig. 1), the Shortland and Haldimand canyons merge mid-slope into a single channel that itself merges downslope with The Gully channel (Fig. 1). The Gully is a prominent, 15 to 20 km wide canyon on the Scotian margin and incises the shelf south-east of Sable Island. Within the canyon, a 1 km wide axial channel widens to 2 km where it emerges from the canyon at 4000 m water depth (Fig. 1). On the levées of the axial channel, sediment waves are observed and diverge southward, forming a slightly erosive valley at 4300 m water depth (CB-W in Fig. 1). To the west, obliquely aligned sediment waves are also observed on an overall gently sloping sea floor (OB in Fig. 1).

At a depth of 4500 m, where the axial channel of The Gully coalesces with the Shortland-Haldimand channel, scarps occur on the channel margins (Fig. 1). Near this location, there is a narrow (*ca* 1 km) axial channel with a knickpoint at its head, which continues to a depth of *ca* 4850 m. Where The Gully and Shortland-Haldimand channels coalesce there is a train of long-wavelength crescentic bedforms on the slightly eroded and flattened sea floor of the western levée (CB-E in Fig. 1).

To the east, an unnamed channel originating from slope-confined canyons evolves downslope. This channel is larger than the above-mentioned ones with widths of 6 to 8 km and is confined to the east by the western levée of the Laurentian Fan. It has a flat bottom and is, in some parts, filled by a large mass transport deposit (MTD) sourced from the western

levée of western Valley (WLWV) of the Laurentian Fan (see Normandeau *et al.* 2018). Large sediment waves on the levée occur to a depth of *ca* 5000 m (LB in Fig. 1).

Shallow stratigraphy and sedimentology of the continental slope

The Neogene seismic stratigraphy of the continental slope consists mainly of high-amplitude parallel reflections overlying discontinuous chaotic reflections, corresponding to late Pliocene sediments overlying Miocene sediments (Piper & Ingram 2003). The upper high-amplitude reflections are locally disrupted by chaotic reflections interpreted as large MTDs. Between the Shortland-Haldimand and unnamed channels, a large MTD (MTD-D) is recognized and was emplaced at *ca* 0.15 Ma BP (Piper & Ingram 2003; Fig. 2). High-amplitude reflections above this MTD are continuous and wavy, interpreted as sediment waves on levées discussed below. The inter-channel regions are mostly composed of these wavy, high-amplitude reflections whereas the channel regions are composed of incoherent to transparent reflections interpreted as sediment infill. Farther downslope, there is a general absence of acoustic penetration with the 3.5 kHz, suggesting the deposition of coarse-grained fan deposits (Fig. 3).

Core 2, collected between The Gully and the unnamed channel (Fig. 1) reveals the nature of the high-amplitude parallel reflections described above (Fig. 4). The upper 300 cm of the core consists of relatively homogeneous mud with faint laminations and rare sandy turbidites (Fig. 4). Graded sandy turbidites become increasingly common at 320 cm; they are mostly millimetre to centimetre thick beds, rarely being thicker than 5 cm and consist of sand-size sediments. Most of the turbidites present in core 2 were deposited between 20 ka cal BP and 17 ka cal BP (Fig. 4, Table 1) and become infrequent in the upper parts of the core. Therefore,

the high-amplitude reflections on the continental slope reflect alternating sandy turbidites and hemipelagites deposited during the late-Pleistocene.

Sediment waves

Long-wavelength crescentic bedforms

Long-wavelength crescentic bedforms are present at two distinct areas offshore of The Gully: (i) directly at the mouth of The Gully (western wavefield) (CB-W in Fig. 1); and (ii) at the confluence of the Shortland-Haldimand channel and Gully channel (eastern wavefield) (CB-E in Fig. 1). In both cases, the bedforms are observed on a net-erosional sector of overbank deposits (Fig. 5A and C).

Long-wavelength crescentic bedforms of the western wavefield are aligned downslope in a semi-continuous train and are confined to a 3 to 7 km wide, 60 to 100 m deep, channel branching westward from The Gully. (Figs 3 and 5A). The main bedforms are observed between depths of 4400 m and 4650 m on a slope of ca 0.4° (Fig. 6D). Their wavelengths and wave heights generally vary between 600 to 2000 m and 10 to 30 m, respectively (Fig. 6A and B). They are asymmetrical downslope, with longer stoss lengths than lee lengths, and with steeper lee sides (2 to 4°) than stoss sides (0.5 to 2.0°) (Fig. 7A). Downstream of the lee side, a deep pool is often observed (Fig. 8).

Slightly larger crescentic bedforms are present at the eastern wavefield (Fig. 5C). Most of these bedforms are located in the upper part of the wavefield but some are separated from others by ≥ 8 km; they typically have wavelengths of 1200 to 4000 m and wave heights of 20 to 30 m (Fig. 6A and B). These bedforms are asymmetrical downslope with stoss and lee slopes of 0.5 to 1.5° and 2 to 4°, respectively.

The 3.5 kHz sub-bottom profiles crossing these two wave fields reveal little acoustic penetration, suggesting the presence of high-impedance coarse sediments (likely to be sand-size according to the turbidites in core 2) (Figs 3 and 7). In some places, slightly stratified reflections are observed towards the crest of the bedforms. Backscatter strengths over the bedforms consist of an alternation of high (\geq -20 dB) to low (\leq -30 dB) intensities on the lee and stoss sides, respectively (Figs 5B to D and 7A). This alternation is consistent over crescentic bedforms (except over the nadir) and suggests that either coarse sediments are preferentially deposited on the lee side while finer sediments are deposited on the stoss side or the that the lee side cuts into the stratigraphy, exposing sandy, previously deposited turbidites.

Bedforms on levées

Bedforms are recognized on the levées of the different channels of the lower slope, most notably on the western levée of the unnamed channel (Figs 1 and 5E). These sediment waves typically have wavelengths of \geq 2000 m and amplitudes as high as 50 m (Fig. 6A and B). Their heights, however, decrease laterally away from the channel, whereas their wavelengths remain similar over the entire wavefield. Therefore, the aspect ratios (λ /H) increase away from the channel. Gradients on the stoss and lee sides are similar at ca 1 to 3° (Fig. 7B).

These bedforms overlie a Quaternary MTD that was emplaced at ca 0.15 Ma BP (MTD-D) (Figs 2 and 9; Piper & Ingram 2003). Since then, their crests have consistently migrated upslope (Fig. 9), with distances of migration between 600 m and 1100 m on ca 0.12 s. two-way travel time (twtt; ca 90 m). Seismic reflection profiles show that the stoss sides form thicker sediment successions than the lee sides, which thin downslope. In some cases, smaller bedforms are superimposed on the stoss side of larger sediment waves (Fig. 9A and B). The

lee side also consists, in some cases, of incoherent reflections, suggesting small-scale slumping which is confirmed by the presence of small arcuate scarps on the multibeam imagery associated with higher backscatter intensities (Fig. 9C and D). The high backscatter values are, however, not consistently located on the lee side of the bedforms since, in some cases, high intensities are located in the trough or even on the stoss side (Fig. 7B).

Oblique bedforms

A series of bedforms located on an open slope, west of The Gully channel, are oblique to the main canyon axis (210° orientation) (OB in Figs 1 and 5G); their obliqueness to the main slope increases downslope. These bedforms are linear, without notable crescentic or sinuous crest shape and are observed on a 0.5° slope (Fig. 6D) between depths of 4300 m and 4800 m. They have wavelengths of ca 1000 m and heights of ca 5 m (Fig. 6A and B) and are generally symmetrical to slightly asymmetrical upslope (Fig. 7C). Their aspect ratios (λ /H) differ considerably from the above-mentioned bedforms, with values >200 (Fig. 6E and F). The stoss and lee side slopes are low, with values of 0 to 0.5° and 0.5 to 1.25° , respectively (Figs 6 and 7C).

The 3.5 kHz sub-bottom profiles collected over these bedforms reveal an acoustic penetration of 0.1 s two-way travel time (twtt; *ca* 75 m), suggesting that they consist of fine-grained sediment (mud) (Fig. 10). The bedforms migrate upslope, over distances of *ca* 200 m for 0.075 s twtt (55 m), which is less than the bedforms observed on the levées. Sub-bottom profiles also show that the sediment succession on the stoss and lee sides is similarly thick with only very little thinning of reflections on the lee side.

DISCUSSION

Origin of sediment waves: Supercritical or subcritical bedforms?

This study provides a unique opportunity to examine three distinct types of deep-water sediment waves that occur within laterally equivalent strata over a relatively confined area of the continental margin (Fig. 3). These sediment waves are large-scale bedforms with mixed relief according to the classification scheme of Symons et al. (2016) (Fig. 6E); they were divided into three types of bedforms due to their location and general shape. Mann-Whitney tests (non-parametric tests used to test differences between two conditions) show, however, that the long-wavelength crescentic bedforms and the levée bedforms share more similar characteristics compared to the oblique bedforms. The aspect ratio of the levée bedforms do not differ significantly from the crescentic bedforms (p = 0.54), although the wavelength and lee slope do (p = 0.004 and p = 0.037, respectively; Fig. 6). In contrast, the aspect ratio, wavelength, height and lee slope of the crescentic and levée bedforms all differ significantly from the oblique bedforms (p < 0.001). The overall slope of the crescentic bedforms does not differ significantly from the oblique bedforms (p = 0.236; Fig. 6). These results suggest that the levée bedforms and the crescentic bedforms may share a similar origin whereas the oblique bedforms may have formed differently. In all three cases, the data indicate that the bedforms migrated upslope, which suggests that they were formed primarily by supercritical turbidity currents (e.g. Symons et al., 2016). Both cyclic steps and antidunes can form under supercritical flows and are known to co-exist (Zhong et al. 2015; Covault et al. 2017) but will interact differently with the overlying current.

Upslope migration of sediment waves has also been shown to form under subcritical turbidity currents in some specific locations and conditions (Kubo & Nakajima, 2003; Hofstra et al. 2018) but are far less common. Subcritical flows generally lead to down-current migration of bedforms (for example, dunes). However, flows are most likely to interact with bedforms in

numerous different ways depending on flow properties (sediment concentration, thickness, velocity, etc.). Therefore, both subcritical and supercritical flows must have been prevalent on the Scotian Slope throughout the Holocene and shaped the overall bedform geometry. Hereafter, it is argued that the main type of flows responsible for the overall geometry and distribution of sediment waves offshore eastern Canada were supercritical or alternating supercritical/subcritical (for example, separated by hydraulic jumps).

Distinguishing antidunes from cyclic steps from morphology and geometry can sometimes be a challenge (Covault et al., 2016). Specific morphologies and internal geometries can nevertheless be used to distinguish one from the other. Net-erosional cyclic steps often exhibit a crescentic shape, which is attributed to faster upslope migration at the centre of the bedform related to its side (Cartigny et al., 2011) and plunge pools at the bottom of the lee side formed by increased erosion at the hydraulic jump (Lee *et al.*, 2002). Net-erosional cyclic steps will form where erosion of a channel is dominant instead of net-accumulation. Net-depositional cyclic steps are characterized by higher aggradation rates, which limit upslope migration compared to net-erosional cyclic steps (Kostic, 2011). Antidunes on the other hand are more symmetrical and short-wavelength bedforms that are sometimes superimposed on the stoss side of longer wavelength cyclic steps (Zhong et al., 2015).

Hereafter, the above criteria are used to argue that, offshore of The Gully Canyon, large-scale cyclic steps formed under turbidity currents whereas antidunes formed under contour-deflected turbidity currents in a mixed turbidite—contourite system.

Net-erosional cyclic steps formed by flow stripping

The downslope asymmetrical long-wavelength crescentic bedforms are similar to neterosional cyclic steps identified in other turbidite systems (Fildani et al. 2006; Lamb et al. 2008; Macdonald et al. 2011; Covault et al. 2014) and appear to migrate upslope based on their crescentic shape and the presence of plunge pools (Fig. 5). Similar but shorterwavelength crescentic bedforms are known to migrate upslope in many submarine canyons (Smith et al., 2007, 2005; Hughes Clarke, 2016; Normandeau et al., 2016, 2014). Although the size of canyon bedforms is orders of magnitude smaller than the deep-water longwavelength bedforms, their similar shape suggests a similar flow/bedform interaction (Symons et al. 2016). The backscatter imagery suggests that their lee sides consist of coarser sediment, or more likely, of exposed previously deposited turbidites (for example, below 300 cm in core 2; Fig. 4), which in turn suggests the erosion of the lee side by higher flow velocities. These inferred coarser grain-sizes, in combination with the crescentic shape, support a cyclic step origin for these sediment waves. The overspilling and stripping flow eroded the levée deposits (Fig. 3), leading to the slight channelization of the bedforms. This erosion of the initial topography indicates erosive flows rather than depositional ones. Additionally, the inferred sand-size of the sediment, evidenced by the absence of 3.5 kHz acoustic penetration, suggests powerful flows that erode the finer component of the sea floor, consistent with the formation of net-erosional cyclic steps. Rapid deceleration of the flow at the bottom of the lee side produces a hydraulic jump, which in turn erodes a relatively deep pool (e.g. Macdonald et al., 2011; Maier et al., 2016) (Fig. 8). The turbidity currents then reaccelerate on the stoss side, where subcritical flows deposit finer sediment (Postma & Cartigny 2014).

The net-erosional cyclic steps to the east are noticeably larger than those to the west. The western field of cyclic steps originates from flow stripping of The Gully channel whereas the

larger ones to the east originate from channels coalescing from the Haldimand-Shortland and the Gully channels. The latter location either suggests that discharge and flow height doubled where channels merged or that the flows originating from the Shortland-Haldimand canyons had a larger discharge than those originating from The Gully. In both cases, it increases the wavelength of the cyclic steps compared to those to the west (Fig. 8) (e.g. Cartigny *et al.*, 2011; Fricke *et al.*, 2015; Normandeau *et al.*, 2016; Zhong *et al.*, 2015).

Net-depositional cyclic steps in overspilling turbidity currents?

Large-scale, upslope migrating rhythmic bedforms observed on the western levée of the unnamed channel (Fig. 5E) formed under turbidity currents and are interpreted to be upperflow regime bedforms although subcritical flows could also have been responsible for their long-term evolution. These bedforms are located downslope of a slight bend in the channel, indicating that flows coming down the slope overspilled on the levée. The symmetry of the bedforms argues in favour of an antidune origin (Cartigny et al. 2011). However, antidunes are generally short-wavelength bedforms (Kostic et al. 2010) whereas the bedforms observed on the levée have the longest wavelengths observed in the area. Cartigny et al. (2011) argued that cyclic steps and antidunes are unlikely to be the same size in a train of sediment waves. Since the bedforms are larger than the net-erosional cyclic steps identified previously, the authors argue in favour of a cyclic step origin. The wavelength of cyclic steps is dependent on flow discharge and thickness (Kostic, 2011); therefore, they would have required a larger flow discharge than the long-wavelength crescentic bedforms to form. Additionally, the presence of smaller upslope migrating sediment waves on the stoss side of the bedforms, suggests the superimposition of shorter wavelength bedforms, possibly antidunes, on longer wavelength ones, a phenomenon often observed in laboratory experiments (Spinewine et al. 2009; Cartigny et al. 2014) and other turbidite systems (Zhong et al. 2015).

Assuming that these bedforms are cyclic steps, they would be strongly aggradational, net-depositional cyclic steps (see Cartigny *et al.*, 2011, fig. 15). Their symmetry is attributed to thicker turbidity currents passing over them, which promote rapid vertical aggradation relative to upstream migration (Kostic 2011). The lee side is composed of slumped material according to the multibeam and backscatter data (Fig. 9) where deposition and erosion are observed in an overall net-aggradational sediment wave. It is, however, worth noting that a large late Pleistocene or Holocene MTD terminates at the channel margin next to these bedforms (Fig. 1), which might have modified the backscatter response and the geometry of some of the sediment waves.

Although the mechanisms responsible for the migration of the overall bedforms appear to be related to supercritical turbidity currents, subcritical currents are likely to occur often and interact differently with the sediment waves. Kubo & Nakajima (2002) showed through numerical simulations that waves can migrate upslope as a result of preferential deposition under a subcritical flow over an initially undulating bottom. Variation in bottom slope can lead to increased deposition on the stoss side, which leads to upslope migration. An initial undulating bottom is required for this model, which suggests that supercritical flows would be responsible for the formation of the initial undulating topography. Subcritical flows are thus unlikely to account for the formation of 1 km long antidunes on the stoss side of some of the waves, which suggests that cyclic steps are responsible for the overall bedform geometry while preferential deposition under subcritical flows can also occur at other times, and result in a similar upslope migrating geometry. Additionally, Kubo & Nakajima (2002) stated that this process is incompatible with extensive sediment wave fields in nature and should only apply to small wave fields (e.g. Hofstra et al., 2018). Therefore, the internal geometry of the bedforms on the levée could be a manifestation of sediment deposition during both subcritical

and supercritical turbidity currents over time, although supercritical conditions probably dominate.

Antidunes formed by contour-deflected turbidity currents

The bedforms oblique to the direction of the channels are fundamentally different from those oriented in the direction of the channels (Figs 6E, 6F and 10), although they both migrate upslope. Their shorter wavelength (800 to 1200 m), fine sediment size and symmetrical geometry suggest that they are antidunes rather than cyclic steps. As with the levée bedforms, subcritical flows are likely to occur, but the low slope gradient of the stoss (0.5°) and the lee side (1.0°) appear unlikely for the origin of preferential deposition during a subcritical flow. Their obliqueness is interpreted here to be the result of turbidity currents that were deflected by contour currents along the Scotian lower slope.

Contour currents are known to produce drift deposits along the Scotian margin and sediment drift growth was greatest during the Late Miocene to Pliocene (Campbell & Mosher, 2016). In the study area, the Gully drift lies under the oblique bedforms and represents a contouritic levée linked to an adjacent channel system, in the sense of Faugères *et al.* (1999). The presence of this drift indicates that the interaction of turbidity currents with westward-flowing bottom currents and the Coriolis force helped construct 1 km long oblique and upslope migrating sediment waves. The predominance of south-westward flows on the lower slope has been inferred by the presence of small-scale bedforms (McCave *et al.* 2002). It has been noted that bottom currents are stronger towards the south-west at depths of 4800 to 5000 m and decrease upslope to tranquil near 4000 m (Swift *et al.* 1985; Tucholke *et al.* 1985). These depths correspond to the location of the antidunes presented in this study (4300 to 4700 m). Bottom current velocities recorded during the early 1980s reveal south-westward speeds of

up to 35 cm s⁻¹ for several days with a maximum of 73 cm s⁻¹ (Richardson *et al.* 1981). Such speeds are sufficient to entrain and transport silt-sized sediment in suspension and to deviate the slower moving top of a turbidity current from its downslope trajectory.

The data presented here suggest that the head and body of turbidity currents coming down the continental slope produced the cyclic steps discussed previously. The flows coming down canyon were first confined and then probably expanded as they travelled downslope (e.g. Symons *et al.*, 2017). The upper parts of the flows, which were composed of finer sediments and were of lower density (e.g. de Leeuw *et al.* 2017) became unconfined and spilled over the channels before being entrained by south-westward-flowing contour currents producing antidunes (Fig. 11). This system would thus be affected by contour currents strong enough to entrain the finest fraction of turbidity currents, but the higher density parts of the flows cannot be deflected to form a fan drift (e.g. Armishaw *et al.*, 2000; Knutz *et al.*, 2002). The entire system would thus be considered a mixed turbidite—contourite system (Mulder *et al.*, 2008) with contouritic levées (Campbell & Mosher, 2016; Faugères *et al.*, 1999).

Behaviour of turbidity currents in a mixed turbidite-contourite system

Numerical modelling parameters

In order to estimate the behaviour of turbidity currents flowing down the Scotian Slope, the numerical model of Cartigny et al. (2011) was used. This numerical model applies gradually varying flow theory to the morphological characteristics of the bedforms, such as the slope and length of the stoss and lee side. This model assumes that sea-floor sediment waves are formed by a cyclic step instability in the turbidity current. If this assumption holds, then the densimetric Froude number (Fr') of the turbidity current varies in a systematic way while flowing over the sediment wave. The model uses these specified variations in Fr' to calculate

the sediment wave geometries that fit hundreds of possible flow conditions. Finally, the sediment waves properties observed on the sea floor are matched to the database of the hundreds of calculated sediment wave properties. The modelled sediment wave that resembles the observed wave geometry most closely is then selected, which is associated with specific flow conditions. See more details in Appendix 1.

Turbidity current behaviour over antidunes is easier to model since simple equations can be used (Hand, 1974); therefore, it is possible to calculate basic flow properties such as flow thickness and flow velocity. Flow thickness (h) is calculated from the wavelength of the bedforms (λ) (Allen 1984):

$$\lambda/4\pi < h < \lambda/2\pi \tag{1}$$

whereas the depth-average flow velocity has previously been estimated successfully using the Hand (1974) equation:

$$U = \{ (g\lambda/2\pi)[(\Delta\rho / (\rho + \rho'))] \}^{1/2}$$
 (2)

where g is the acceleration of gravity, $\Delta \rho$ is the density contrast across the interface, ρ is the density of the flow and ρ' is the density of the ambient fluid.

Turbidity current behaviour based on the numerical model

The net-depositional cyclic steps on the levée were difficult to model numerically because the predicted length and amplitude of the bedforms did not directly match some of the observations. This could be due to the fact that the morphology of the bedforms was modified by a late-Pleistocene/Holocene landslide that terminated against them (Normandeau *et al.*, 2018). Using the bedforms located upslope of the large landslide, the flow behaviour can be estimated over the levée. The turbidity currents probably had a discharge of 200 to 300 m³ s⁻¹ at a velocity of 5 to 7 m s⁻¹. They were thick, with heights of 30 to 60 m before the

hydraulic jump and 90 to 180 m following the hydraulic jump, which is consistent with 1 km long antidune formation on the stoss side (80 to 160 m according to Eq. 1). These flow heights are compatible with more symmetrical and net-depositional cyclic steps on levées since thicker flows are needed to produce more symmetrical, strong aggradational cyclic steps (e.g. Kostic, 2011). These thick flows largely overspilled the channels, supplying coarse sediment on open slopes responsible for the presence of sandy turbidites at 4000 m water depth (Fig. 4).

Over the net-erosional cyclic steps (long-wavelength crescentic bedforms), the Froude number predicted by the model is estimated at 2 on the lee side with the flow velocity ranging between 3 m and 6 m s⁻¹ (Fig. 11). The discharge varies between 250 m³ and 300 m³ s⁻¹ with a flow height of *ca* 10 to 30 m. Such flows would be associated with 1.0 to 2.5 m s⁻¹ velocities and 30 to 80 m thick flows downstream of the hydraulic jump, on the stoss side. The relief of the channel is between 100 m at the upstream part and 50 m in the downstream part where the net-erosional cyclic steps are located. The flow heights indicate that the fast-flowing component of the flow was confined within the slightly channelized region whereas the lower velocity component, where the flow height increases to 30 to 80 m, has the potential to overspill over the levée by 20 to 30 m. This overspilling part of the flow was thus deflected by south-westward contour currents and is likely to have produced the oblique antidunes.

Over the antidunes, minimum and maximum flow thicknesses of 80 m and 160 m are estimated based on Eq. 1. For these flows to form, the overspilling part of the turbidity currents over the long-wavelength crescentic bedforms, which initially overspilled by 20 to 30 m, would require an increase in height, probably by water entrainment, during their deflection by contour currents. Such initial flow thickness would be too thin to produce the antidunes. Therefore, contour currents probably mix the upper parts of the flow, leading to

significant flow dilution and increased thickness on the open slope, resulting in lower velocities and Fr', which is then responsible for forming the antidunes. Alternatively, the flows responsible for the antidunes can be thicker than those modelled and be deflected westward. These larger flows could then interact differently with the long-wavelength crescentic bedforms.

Assuming flow density ranging from >0 to 5 kg m⁻³ (0 to 0.5%_{vol}), the turbidity current flow velocity over the antidunes would vary between >0 and 2 m s⁻¹ (Fig. 11). A recent giant turbidity current triggered in 1929 was estimated to travel down-canyon in the region with sediment concentration of 4.7 to 5.4%_{vol.} but more likely with <1%_{vol} in the upper parts (Stevenson et al., 2018). Turbidity currents recorded in the Congo Canyon on the other hand were measured at 0.1% vol concentration (Azpiroz-Zabala et al., 2017). Assuming that the dilute contour-deflected turbidity currents would have smaller sediment concentration than the dilute Congo Canyon flows, the combined (contour and turbidity current) velocities would have been ≤1 m s⁻¹ over the antidunes. For these flows to be responsible for the antidunes, the flows coming down the channel need to be thicker than the initial overspilling flow that form the cyclic steps. Therefore, if an initial 0.1%_{vol} concentration at the top of the flow being diluted three times to reach the minimum thickness required is assumed, a concentration of 0.03%_{vol} would lead to flows of about ≤0.5 m s⁻¹. Alternatively, some flows coming down The Gully Canyon could be thicker than predicted by the model and be deflected westward. The low sediment concentration values are compatible with the interpreted dilute turbidity currents deflected by contour currents.

Controls on bedform distribution in a mixed turbidite/contourite system

Gradient plays a critical role on supercritical flows and the formation of bedforms (Zhong *et al.* 2015; Maier *et al.* 2017). However, in some cases, such as offshore The Gully Canyon, other factors appear to play a more important role on determining the type of bedforms created since they all form on a similar gradient ($ca \ 0.5^{\circ}$). The modelling of the flows over the bedforms in this study reveals that cyclic steps form under flows of 3 to 6 m s⁻¹, which are faster than the flows over the antidunes ($\leq 1 \text{ m s}^{-1}$). Since gradients are similar overall, other flow properties must be in play to reduce velocity and Fr' number from 2 to 4 (cyclic steps) to 1 (antidunes).

Turbidity currents breaching the levées of The Gully channel have high velocities and high Fr' numbers that enable the formation of cyclic steps. Turbidity current thickness increases to 30 to 80 m on the stoss side, following the hydraulic jump (Fig. 11). At that location, contour currents are capable of deflecting the upper dilute part of the flow westward. The flow velocity and flow thickness modelling of the antidunes illustrates that contour-deflected turbidity currents are slower and thicker (80 to 160 m). The thicker flows may be explained by mixing caused by the interaction of turbidity currents and contour currents displacing and overspilling the flows westward. Since the overall slope of antidunes is similar to that of the cyclic steps, gradient cannot explain the lower velocities and Fr' number. Therefore, the authors suggest that lower sediment concentration of the flow reduced the flow velocity, thereby reducing Fr' to ca 1, which allowed the formation of antidunes. Additionally, Balmforth & Vakil (2012) have shown that cyclic steps require a certain amount of sea floor erosion to form, which does not appear to be the case for the antidunes presented here (Fig. 10). Overspilling flow deflected by contour currents may no longer be capable of eroding the sea floor and, therefore, would not be able to build cyclic steps. The obliqueness of the antidunes (20 to 25° to local slope) nevertheless indicates that the relative influence of

turbidity currents is stronger than contour currents. The latter are only strong enough to deflect the turbidity currents and modify their path, resulting in the mixed turbidite—contourite system with contouritic levées (Campbell & Mosher, 2016; Faugères *et al.*, 1999).

The role of cyclic steps in channel inception

Fildani et al. (2013) argued that channel inception is possible during an early phase of erosion by turbidity currents. This early phase of erosion is then followed by aggradation that constructs levées, which subsequently confine the flows. Conversely, de Leeuw et al. (2016) demonstrated, through experimental work, that channel inception was possible by depositional and erosional turbidity currents on a featureless slope where formation of levées channelized subsequent flows. The geomorphology of The Gully region supports the hypothesis of Fildani et al. (2013) that channel inception is mainly achieved by an initial phase of erosion. The net-erosional cyclic steps (long-wavelength crescentic bedforms) are located where flow stripping occurs (Fig. 11). This location is similar to flow stripping in Monterey submarine canyon (Fildani et al. 2006) or on the Lucia Chica channel system, USA (Maier et al. 2011, 2013). The slight channelization of the net-erosional cyclic steps suggests that they formed during an early erosional phase and that they represent incipient channels. The net-erosional cyclic steps are thus interpreted to be relatively young when compared to The Gully channel. The authors speculate that these incipient channels might have formed during the late stages of glaciation, when turbidity current activity was at its maximum. On the lower slope, this period appears to have been between 20 ka and 17 ka cal BP (Fig. 4). Since the retreat of the ice sheet in the region >17 ka cal BP (Shaw et al., 2006), few turbidity currents reach submarine fans (Fig. 4). Therefore, a future period of turbidity current activity will be required to further build confined channels.

CONCLUSION

On the Scotian Slope, The Gully channel system merges with other submarine channels, on which formed three distinct types of bedforms: long-wavelength crescentic bedforms, bedforms on levées and oblique bedforms on open slopes. These different types of bedforms reveal the relative influence of turbidity currents versus contour currents on the formation and distribution of sediment waves:

- (i) Long-wavelength crescentic bedforms, interpreted as net-erosional cyclic steps, are located where flow stripping occurs, indicating powerful flows (3 to 6 m s⁻¹) eroding the sea floor.
- (ii) Net-depositional cyclic steps are located on the levée of channels, where depositional processes are greater than erosional processes. The flows responsible for these bedforms are thicker and fast (5 to 7 m s⁻¹), promoting rapid vertical aggradation.
- (iii) In contrast, antidunes are oriented obliquely to the main turbidity current direction, indicating that the flows responsible for their presence were deflected by contour currents. The upper dilute part of turbidity currents were entrained by contour currents and formed low-relief, 1 km wavelength antidunes.

The deflection of the turbidity currents by contour currents was possible because of upper flow thickening and water entrainment. The upper, dilute part of turbidity currents was entrained westward and further thickened due to mixing with contour currents. This mixing led to a decrease in sediment concentration, which probably lowered flow velocities, thereby lowering the Fr' number and producing oblique antidunes. This study thus provides a clear example of the behaviour of turbidity currents being deflected by contour currents on the lower continental slope, at >4000 m water depth, thus controlling the distribution of upperflow regime bedforms.

ACKNOWLEDGEMENTS

The authors would like to thank the crew members of *R/V Atlantis* and *CCGC Hudson* during cruises AT22-1 and 2016011Phase1 for help during data acquisition. We are grateful to Nicolas Van Nieuwenhove for the picking and identification of foraminifera, David J.W. Piper and Kimberley Jenner for constructive comments on a preliminary version of this manuscript. Aaron Fricke and Chris Stevenson provided thorough and constructive reviews that improved the quality of this paper. Support for this project was from the Geological Survey of Canada.

REFERENCES

- **Allen J.R.L.** (1984) Sedimentary Structures, Their Character and Physical Basis, Elsevier.

 Amsterdam.
- **Armishaw J.E., Holmes R.W.** and **Stow D.A.V.** (2000) The Barra Fan: A bottom-current reworked, glacially-fed submarine fan system. *Mar Pet Geol*, **17**,219–238
- Azpiroz-Zabala M, Cartigny MJB, Talling PJ, Parsons, D.R., Sumner, E.J., Clare, M.A., Simmons, S.M., Cooper, C. and Pope, E.L. (2017) Newly recognized turbidity current structure can explain prolonged flushing of submarine canyons. *Sci Adv*, 3:e1700200. doi: 10.1126/sciadv.1700200
- **Balmforth N.** and **Vakil A.** (2012) Cyclic steps and roll waves in shallow water flow over an erodible bed. *J Fluid Mech*, **395**, 35–62 . doi: 10.1017/jfm.2011.555
- Campbell D.C. and Mosher D.C. (2016) Geophysical evidence for widespread Cenozoic bottom current activity from the continental margin of Nova Scotia, Canada. *Mar Geol*, 378, 237–260. doi: 10.1016/j.margeo.2015.10.005
- Campbell D.C. and Normandeau A. (2018) CCGS Hudson Expedition 2016-011, phase 1.

 Marine geohazards and seabed processes along the lower Scotian Slope, June 2-14,

 2016. Geological Survey of Canada Open File Report 8346, 55 p. doi: 10.4095/306450
- Cartigny M.J.B., Postma G., van den Berg J.H. and Mastbergen D.R. (2011) A comparative study of sediment waves and cyclic steps based on geometries, internal structures and numerical modeling. *Mar Geol*, **280**, 40–56. doi: 10.1016/j.margeo.2010.11.006
- Cartigny M.J.B., Ventra D., Postma G. and van den Berg, J.H. (2014) Morphodynamics and sedimentary structures of bedforms under supercritical-flow conditions: New insights from flume experiments. *Sedimentology*, **61**,712–748. doi: 10.1111/sed.12076

- **Casalbore D., Romagnoli C., Bosman A., Chiocci F.L.** (2014) Large-scale seafloor waveform on the flanks of insular volcanoes (Aeolian Archipelago, Italy), with inferences about their origin. *Mar. Geol.*, **355**, 318-329.
- Covault J.A., Kostic S., Paull C.K., Ryan, H.F. and Fildani, A. (2014) Submarine channel initiation, filling and maintenance from sea-floor geomorphology and morphodynamic modelling of cyclic steps. *Sedimentology*, **61**, 1031–1054. doi: 10.1111/sed.12084
- Covault J.A., Kostic S., Paull C.K., Sylvester, Z. and Fildani, A. (2017) Cyclic steps and related supercritical bedforms: Building blocks of deep-water depositional systems, western North America. *Mar Geol*, **393**, 4–20 . doi: 10.1016/j.margeo.2016.12.009
- de Leeuw J., Eggenhuisen J.T. and Cartigny M.J. (2016) Morphodynamics of submarine channel inception revealed by new experimental approach. *Nat Commun*, **7**, 10886. doi: 10.1038/ncomms10886
- **de Leeuw J., Eggenhuisen J.T.** and **Cartigny M.J.B.** (2017) Linking submarine channel-levée facies and architecture to flow structure of turbidity currents; insights from flume tank experiments. *Sedimentology*. doi: 10.1111/sed.12411
- Ercilla G., Wynn R.B., Alonso B. and Baraza J. (2002) Initiation and evolution of turbidity current sediment waves in the Magdalena turbidite system. *Mar Geol*, **192**, 153–169
- **Faugères J.C., Stow D.A.V., Imbert P., Viana A.** (1999) Seismic features diagnostic of contourite drifts. *Mar Geol*, **162**, 1–38. doi: 10.1016/S0025-3227(99)00068-7
- Fildani A., Hubbard S.M., Covault J.A., Maier K.L., Romans B.W., Traer M., and Rowland J.C. (2013) Erosion at inception of deep-sea channels. *Mar Pet Geol*, 41, 48–61. doi: 10.1016/j.marpetgeo.2012.03.006
- **Fildani A., Normark W.R., Kostic S., Parker G.** (2006) Channel formation by flow stripping: large-scale scour features along the Monterey East Channel and their relation

- to sediment waves. *Sedimentology*, **53**, 1265–1287 . doi: 10.1111/j.1365-3091.2006.00812.x
- **Flood R.D.** (1988) A lee wave model for deep-sea mudwave activity. *Deep Sea Res*, **35**, 973–983
- Fortin D., Francus P., Gebhardt A.C., Hahn A., Kliem P., Lisé-Pronovost A.,

 Roychowdhury R., Labrie J., St-Onge G. and PASADO science team. (2013)

 Destructive and non-destructive density determination: Method comparison and evaluation from the Laguna Potrok Aike sedimentary record. Quat. Sci. Rev., 71, 147-153
- Fricke A., Sheets B.A., Nittrouer C.A., Allison M.A., and Ogston A.S. (2015) An examination of Froude-supercritical flows and cyclic steps on a subaqueous lacustrine delta, Lake Chelan, Washington, USA. *J. Sed. Res.*, **85**, 754-767.
- **Hofstra, M., Peakall, J., Hodgson, D. M.,** and **Stevenson, C. J.** (2018) Architecture and morphodynamics of subcritical sediment waves in an ancient channel—lobe transition zone. *Sedimentology*.
- Gong C., Wang Y., Peng X., Li W., Yan Q. and Xu, S. (2012) Sediment waves on the South China Sea Slope off southwestern Taiwan: Implications for the intrusion of the Northern Pacific Deep Water into the South China Sea. *Mar Pet Geol*, 32, 95–109. doi: 10.1016/j.marpetgeo.2011.12.005
- Gong C., Wang Y., Xu S., Pickering K.T., Peng X., Li W. and Yan Q.(2015) The northeastern South China Sea margin created by the combined action of down-slope and along-slope processes: Processes, products and implications for exploration and paleoceanography. *Mar Pet Geol*, **64**, 233–249 . doi: 10.1016/j.marpetgeo.2015.01.016
- Gonthier E, Faugères JC, Viana A, et al (2003) Upper Quaternary deposits on the Sao

- Tomé deep-sea channel levee system (South Brazilian Basin): major turbidite versus contourite processes. Mar Geol 199:159–180. doi: 10.1016/s0025-3227(03)00128-2
- **Hughes Clarke J.E.** (2016) First wide-angle view of channelized turbidity currents links migrating cyclic steps to flow characteristics. *Nat Commun*, **7**, 11896. doi: 10.1038/ncomms11896
- Jenner K.A., Piper D.J.W., Campbell D.C. and Mosher D.C. (2007) Lithofacies and origin of late Quaternary mass transport deposits in submarine canyons, central Scotian Slope, Canada. *Sedimentology*, **54**, 19–38. doi: 10.1111/j.1365-3091.2006.00819.x
- Knutz P.C., Jones E.J.W., Austin W.E.N. and Van Weering T.C.E. (2002) Glacimarine slope sedimentation, contourite drifts and bottom current pathways on the Barra Fan, UK North Atlantic margin. *Mar Geol*, 188, 129–146. doi: 10.1016/S0025-3227(02)00278-5
- **Kostic S.** (2011) Modeling of submarine cyclic steps: Controls on their formation, migration, and architecture. *Geosphere*, **7**, 294–304 . doi: 10.1130/ges00601.1
- **Kostic S., Sequeiros O., Spinewine B.** and **Parker G.** (2010) Cyclic steps: A phenomenon of supercritical shallow flow from the high mountains to the bottom of the ocean. *J Hydro-environment Res*, **3**, 167–172 . doi: 10.1016/j.jher.2009.10.002
- **Kubo Y.** and **Nakajima T.** (2002) Laboratory experiments and numerical simulation of sediment-wave formation by turbidity currents. *Mar Geol*, **192**, 105–121 . doi: 10.1016/S0025-3227(02)00551-0
- Lamb M.P., Parsons J.D., Mullenbach B.L., Finlayson D.P., Orange D.L. and Nittrouer C.A. (2008) Evidence for superelevation, channel incision, and formation of cyclic steps by turbidity currents in Eel Canyon, California. *Geol Soc Am Bull*, 120, 463–475. doi: 10.1130/b26184.1

- Lee S.E., Talling P.J., Ernst G.G.J., and Hogg A.J. (2002) Occurrence and origin of submarine plunge pools at the base of the US continental slope. *Mar Geol*, **185**, 363-377.
- Macdonald H.A., Wynn R.B., Huvenne V.A.I., Peakall J., Masson D.G., Weaver P.P.E and McPhail S.D. (2011) New insights into the morphology, fill, and remarkable longevity (>0.2 m.y.) of modern deep-water erosional scours along the northeast Atlantic margin. *Geosphere*, **7**, 845–867. doi: 10.1130/GES00611.1
- Maier K.L., Brothers D.S., Paull C.K., McGann M., Caress D.W. and Conrad J.E.

 (2017) Records of continental slope sediment flow morphodynamic responses to gradient and active faulting from integrated AUV and ROV data, offshore Palos Verdes, southern California Borderland. *Mar Geol*, 393, 47–66. doi: 10.1016/j.margeo.2016.10.001
- Maier K.L., Fildani A., Paull C.K., Graham S.A., McHargue T.R., Caress D.W. and McGann M. (2011) The elusive character of discontinuous deep-water channels: New insights from Lucia Chica channel system, offshore California. *Geology*, 39, 327–330. doi: 10.1130/g31589.1
- Maier K.L., Fildani A., Paull C.K., McHargue T.R., Graham S.A. and Caress D.W. (2013) Deep-sea channel evolution and stratigraphic architecture from inception to abandonment from high-resolution Autonomous Underwater Vehicle surveys offshore central California. *Sedimentology*, **60**, 935–960 . doi: 10.1111/j.1365-3091.2012.01371.x
- Marshall N.R., Piper D.J.W., Saint-Ange F. and Campbell D.C. (2014) Late Quaternary history of contourite drifts and variations in Labrador Current flow, Flemish Pass, offshore eastern Canada. *Geo-Marine Lett*, **34**,457–470 . doi: 10.1007/s00367-014-0377-z

- Masson D.G., Howe J.A. and Stoker M.S. (2002) Bottom-current sediment waves, sediment drifts and contourites in the northern Rockall Trough. *Mar Geol*, **192**, 215–237. doi: 10.1016/S0025-3227(02)00556-X
- McCave I.N., Chandler R.S., Swift S.A. and Tucholke B.E. (2002) Contourites of the Nova Scotian continental rise and the HEBBLE area. In: Stow DA V, Pudsey CJ, Howe JA, *et al.* (eds) Deep-Water Contourite Systems: Modern Drifts and Ancient Series, Seismic and Sedimentary Characteristics. The Geological Society of London, pp 21–38
- **Migeon S., Savoye B.** and **Faugeres J.C.** (2000) Quaternary development of migrating sediment waves in the Var deep-sea fan: Distribution, growth pattern, and implication for levee evolution. *Sediment Geol*, **133**, 265–293. doi: 10.1016/S0037-0738(00)00043-9
- Mosher D.C., Piper D.J.W., Campbell D.C. and Jenner K.A. (2004) Near-surface geology and sediment-failure geohazards of the central Scotian Slope. *Am Assoc Pet Geol Bull*, **88**, 703–723. doi: 10.1306/01260403084
- **Mulder T., Faugères J.C.** and **Gonthier E.** (2008) Chapter 21 Mixed Turbidite-Contourite Systems. Dev Sedimentol 60:435–456. doi: 10.1016/S0070-4571(08)10021-8
- Nakajima T., Satoh M. and Okamura Y. (1998) Channel-levee complexes, terminal deep-sea fan and sediment wave fields associated with the Toyama Deep-Sea Channel system in the Japan Sea. *Mar Geol*, **147**, 25–41
- Normandeau A., Campbell D.C., Piper D.J.W. and Jenner K.A. (2018) New evidence for a major late-Quaternary submarine landslide on the external western levee of Laurentian Fan. *Geol Soc Spec Publ*
- Normandeau A., Lajeunesse P., Poiré A.G. and Francus P. (2016) Morphological expression of bedforms formed by supercritical sediment density flows on four fjord-

- lake deltas of the south-eastern Canadian Shield (Eastern Canada). *Sedimentology*, **63**, 2106–2129. doi: 10.1111/sed.12298
- Normandeau A., Lajeunesse P., St-Onge G., Bourgault D., St-Onge Drouin S.,

 Senneville S. and Bélanger S. (2014) Morphodynamics in sediment-starved inner-shelf submarine canyons (Lower St. Lawrence Estuary, Eastern Canada). *Mar Geol*, 357, 243–255. doi: 10.1016/j.margeo.2014.08.012
- Normark W.R., Hess G.R., Stow D.A.V. and Bowen A.J. (1980) Sediment waves on the Monterey fan levee: a preliminary physical interpretation. *Mar Geol*, **37**, 1–18
- **Parker G.** (1996) Some Speculations on the Relation Between Channel Morphology and Channel-scale Flow Structures. *Coherent flow Struct open channels*, **423**, 424–458
- **Pickart R.S.** (1992) Water mass components of the North Atlantic deep western boundary current. *Deep Sea Res Part I Ocean Res*, **39**, 1553–1572. doi: 10.1016/0198-0149(92)90047-W
- **Piper D.J.W.** (2005) Late Cenozoic evolution of the continental margin of eastern Canada.

 Nor J Geol, 85, 305–318
- **Piper D.J.W.** (1987) Glaciomarine sedimentation on the continental slope off eastern Canada. *Geosci Canada*, **15**, 23–28
- **Piper D.J.W.** and **Ingram S.** (2003) Geological Survey of Canada Major Quaternary sediment failures on the east Scotian Rise, eastern Canada. *Curr Res Geol Surv Canada* 1–7
- Piper D.J.W. and Normark W.R. (1989) Late Cenozoic sea-level change and the onset of glaciation: impact on continental slope progradation off eastern Canada. *Mar Pet Geol*, 6, 336–347

- **Postma G.** and **Cartigny M.J.B.** (2014) Supercritical and subcritical turbidity currents and their deposits--A synthesis. *Geology*, **42**, 987–990. doi: 10.1130/g35957.1
- **Rebesco M., Hernández-Molina F.J., Van Rooij D.** and **Wåhlin A.** (2014) Contourites and associated sediments controlled by deep-water circulation processes: State-of-the-art and future considerations. *Mar Geol*, **352**, 111–154. doi: 10.1016/j.margeo.2014.03.011
- Reimer P.J., Bard E., Bayliss A., Beck J.W., Blackwell P.G., Ramsey C.B., Buck C.E., Cheng H., Edwards R.L., Friedrich M., Grootes P.M., Guilderson T.P., Haflidason H., Hadjas I., Hatté C., Heaton T.J., Hoffman D.L., Hogg A.G., Hughen K.A., Kaiser K.F., Kromer B., Manning S.W., Niu M., Reimer R.W., Richards D.A., Scott E.M., Southon J.R., Staff R.A., Turney C.S.M., and van der Plicht J. (2013) Intcal13 and Marine13 radiocarbon age calibration curves 0–50,000 years cal. B.P.: Radiocarbon, 55, 1869–1887. doi:10.2458/azu_js_rc.55.16947.
- **Ribó M., Puig P., Muñoz A., Iacono C.L., Masqué P., Palanques, A., Acosta J., Guillen J.** and **Ballesteros M.G.** (2016) Morphobathymetric analysis of the large fine-grained sediment waves over the Gulf of Valencia continental slope (NW Mediterranean). *Geomorphology*, **253**, 22–37. doi: 10.1016/j.geomorph.2015.09.027
- **Richardson M.J., Wimbush M.** and **Mayer L.** (1981) Exceptionally strong near-bottom flows on the continental rise of nova scotia. *Science*, **213**, 887–8. doi: 10.1126/science.213.4510.887
- Shaw J., Piper D.J.W., Fader G.B.J., King E.L., Todd B.J., Bell T., Batterson M.J. and Liverman D.G.E. (2006) A conceptual model of the deglaciation of Atlantic Canada. *Quat. Sci. Rev.*, **25**, 2059-2081.
- Smith D.P., Kvitek R., Iampietro P.J. and Wong K. (2007) Twenty-nine months of geomorphic change in upper Monterey Canyon (2002–2005). *Mar Geol*, **236**, 79–94.

- Smith D.P., Ruiz G., Kvitek R. and Iampietro P.J. (2005) Semiannual patterns of erosion and deposition in upper Monterey Canyon from serial multibeam bathymetry. *Geol Soc Am Bull*, **117**, 1123–1133 . doi: 10.1130/b25510.1
- Spinewine B., Sequeiros O.E., Garcia M.H., Beaubouef R.T., Sun T., Savoye B. and Parker G. (2009) Experiments on Wedge-Shaped Deep Sea Sedimentary Deposits in Minibasins and/or on Channel Levees Emplaced by Turbidity Currents. Part II. Morphodynamic Evolution of the Wedge and of the Associated Bedforms. *J Sediment Res*, 79, 608–628. doi: 10.2110/jsr.2009.065
- **Stow D.A.V.** and **Faugères J.C.** (2008) Chapter 13 Contourite Facies and the Facies Model. *Dev Sedimentol*, **60**, 223–256. doi: 10.1016/S0070-4571(08)10013-9
- **Stuiver M., and Reimer P.J.** (1993) Extended 14C data- base and revised Calib 3.0 14C age calibration program: *Radiocarbon*, **35**, 215–230. doi:10.1017/S0033822200013904.
- **Swift S.A., Hollister C.D.** and **Chandler R.S.** (1985) Close-up stereo photographs of abyssal bedforms on the Nova Scotian continental rise. *Mar Geol*, **66**, 303–322 . doi: 10.1016/0025-3227(85)90036-2
- **Sylvester Z., Pirmez C.** and **Cantelli A.** (2011) A model of submarine channel-levee evolution based on channel trajectories: Implications for stratigraphic architecture. *Mar Pet Geol*, **28**, 716–727 . doi: 10.1016/j.marpetgeo.2010.05.012
- Symons W.O., Sumner E.J., Paull C.K., Cartigny M.J.B., Xu J.P., Maier K.L., Lorenson T.D. and Talling P.J. (2017) A new model for turbidity current behavior based on integration of flow monitoring and precision coring in a submarine canyon. *Geology*, **45**, 367–370. doi: 10.1130/G38764.1
- Symons W.O., Sumner E.J., Talling P.J., Cartigny M.J.B. and Clare M.A. (2016) Large-This article is protected by copyright. All rights reserved.

- scale sediment waves and scours on the modern seafloor and their implications for the prevalence of supercritical flows. *Mar Geol*, **371**, 130–148. doi: 10.1016/j.margeo.2015.11.009
- **Tucholke B.E., Hollister C.D., Biscaye P.E.** and **Gardner W.D.** (1985) Abyssal current character determined from sediment bedforms on the Nova Scotian continental rise. *Mar Geolo*, **66**, 43–57
- Urgeles R., De Mol B., Puig P., De Batist M. and Hughes Clarke J.E. (2009) Sediment undulations on the Llobregat prodelta: Signs of early slope instability or sedimentary bedforms? *Rend Online Soc Geol Ital*, **7**, 103–106. doi: 10.1029/2005JB003929
- **Wade J.A.** and **MacLean B.C.** (1990) The geology of the southeastern margin of Canada. Geol Cont margin East Canada Geol Surv Canada, *Geol Canada*, **2**, 167–238
- **Wynn R.B.** and **Stow D.A.V.** (2002) Classification and characterisation of deep-water sediment waves. *Mar Geol*, **192**, 7–22
- **Zhong G., Cartigny M.J.B., Kuang Z.** and **Wang L.** (2015) Cyclic steps along the South Taiwan Shoal and West Penghu submarine canyons on the northeastern continental slope of the South China Sea. *Geol Soc Am Bull*, **127**, 804–824. doi: 10.1130/b31003.1

FIGURES AND TABLES

- **Table 1:** Radiocarbon age information for core 2016011PH1-0002.
- Fig. 1 Location of study area, offshore The Gully, Shortland, Haldimand and an unnamed canyon. LF: Laurentian Fan. ULSW: Upper Labrador Sea Water. CLSW: Classic Labrador Sea Water (CLSW). DSOW: Denmark Strait Overflow Water ISOW: Iceland-Scotland Overflow Water (ISOW). OB: Oblique bedforms. CB: Crescentic bedforms. LB: Levée bedforms.
- **Fig. 2:** Seismic stratigraphy of the lower continental slope of the outer Gully region. It comprises high-amplitude parallel reflections disturbed by mass-transport deposits (MTD). MTD-D was dated *ca* 0.15 Ma BP (Piper & Ingram 2003) while the uppermost MTD is late-Pleistocene or Holocene in age (see Normandeau *et al.* 2018).
- **Fig. 3:** Geomorphological and stratigraphic context of the bedforms over the outer Gully region. Note the absence of acoustic penetration under the crescentic bedforms compared to the presence of parallel high-amplitude reflections where the oblique bedforms are located.
- **Fig. 4**: CT-Scan and core lithology of core 2016011PH1-02 illustrating numerous turbidites associated with the formation of sediment waves in the region. Location of core in Fig. 1.
- **Fig. 5:** Multibeam bathymetry and backscatter imagery of the four main sediment wave fields: multibeam (A) and backscatter (B) imagery of the western wavefield of crescentic bedforms; multibeam (C) and backscatter (D) imagery of the eastern wavefield of crescentic bedforms; multibeam (E) and backscatter (F) imagery of the bedforms on levées; multibeam (G) and backscatter (H) imagery of the oblique bedforms.

- **Fig. 6**: Morphological properties of the bedforms: (A) wavelength; (B) height; (C) lee slope; (D) bedform slope; (E) aspect ratios compared to Symons *et al.* (2016); (F) aspect ratio versus slope compared to a summary of bedforms from Dietrich *et al.* (2016). Mann-Whitney tests were performed between the levée bedforms, the crescentic bedforms and the oblique bedforms and are presented on (A) to (D) and (F). A p-value of <0.05 indicates that the morphological properties differ significantly between the bedforms.
- **Fig. 7:** Profiles of the three main types of bedforms and their associated slopes and backscatter strength. (A) Crescentic bedforms (net-erosional cyclic steps). (B) Bedforms on levées (net-depositional cyclic steps. (C) Oblique bedforms (antidunes). See Fig. 5 for locations.
- **Fig. 8:** A 3.5 kHz sub-bottom profile crossing the crescentic bedforms. The absence of acoustic penetration indicates the coarse nature of the sediment waves. See Fig. 5 for location.
- **Fig. 9:** Seismic reflection profiles of the bedforms on the levée of the channel illustrating upslope migration and the presence of smaller wavelength sediment waves on the stoss side. Note the chaotic reflections on the lee side of some of the bedforms. (A) Huntec DTS profile. (B) GI-Gun profile. (C) Multibeam imagery of lee side slumping evidenced in the seismic profiles. (D) Backscatter imagery of lee-side slumping illustrating the high intensity downslope of small scarps.
- **Fig. 10:** A 3.5 kHz sub-bottom profile illustrating the upslope migration of the oblique bedforms, interpreted as antidunes. Note that the entire sedimentary package drapes the underlying reflections conformably on the stoss and the lee side.
- **Fig. 11:** (A) Conceptual model of turbidity currents flowing downslope, illustrating the channel inception by flow stripping and the formation of cyclic steps, the deflected low

density turbidity currents forming antidunes and the overspilling turbidity currents forming cyclic steps on the levee of the channels. Flow behaviour over antidunes (B), net-erosional cyclic steps (C) and net depositional cyclic steps (D) are also presented.

Table 1

Core number	Depth in core (cm)	Material dated	¹⁴ C age (yr вр)	Median calibrated age (cal вр)	Laboratory number
2016011PH1-02	381-384	Planktonic foraminifera (Nps)	14565 ± 35	17242 (17074-17433)	UCIAMS 198678
2016011PH1-02	571-574	Mixed planktonic foraminifera	16695 ± 40	19661 (19506-19866)	UCIAMS 198679

MODELLING APPENDIX

This appendix provides a quick overview of a gradually varying flow model that links sediment waves geometries to flow properties (Cartigny et al., 2011).

Key assumptions in the model

- 1. This model calculates sediment wave geometries under the assumption that they are formed by a cyclic step instability. It calculates a flow that would generate a similar sediment wave if this flow was going through a cyclic step instability. However, this model not prove that the sediment wave is formed by a cyclic step instability.
- 2. The model assumes that the flows vary in thickness or velocity gradually over long distances.
- 3. The model assumes that there is no exchange of sediment between the flow and the sea floor; there is no erosion or deposition at the base of the flow. Additionally, the model does not include water entrainment or detrainment between the flow and the ambient water.
- 4. The model assumes that the friction in between the sea floor and the flow is determined by relative roughness of the sea floor and the Reynolds number of the flow (Colebrook & White, 1937). The friction in between the flow and the ambient water is here set to 0.33 times the friction at the base following experimental work by Masterbergen & Van Den Berg (2003).

Densimetric Froude number variation due to a cyclic step instability

If the sediment waves are formed by a cyclic step instability, then the trough of the sediment wave will host a hydraulic jump. A hydraulic jump forms an abrupt transition between an

upstream supercritical flow (Fr' > 1) and a downstream subcritical flow (Fr' < 1). In between the troughs the flow will systematically increase its Fr' to return from the subcritical value upstream to the supercritical value downstream. Additionally, a cyclic step interpretation also dictates that the Fr' on the crest of the sediment wave will be around unity. Furthermore, every Fr' number before the hydraulic jump is uniquely linked a specific Fr' after the hydraulic jump. These couples of linked Fr' are called conjugate Fr'. As a result, selecting a pre-jump Fr' will determine the post-jump Fr'. These two conjugate Fr's and the Fr' = 1 at the crest form the boundary conditions of the model.

Model set-up

Step 1: Collect geometrical data from the sea-floor sediment wave

The first step is to select the sediment wave on the sea-floor data for which the reconstruction is made. This could either be an individual sediment wave, or it could be an average of a set of similar sediment waves. Once the sediment wave of interest is selected, the length and gradients of both the stoss and the lee sides needs to be determined.

Step 2: Select a wide range of flow properties that are likely to occur on the sea floor

The model is an inverse model, implying that it will run for many different flow properties. Each of these flow properties will produce a different sediment wave geometry. After running all of the modelling, the calculated sediment wave that most strongly resemble the sea-floor sediment wave is selected.

The model characterizes a flow by three variables: (i) the supercritical Fr' just upstream of the hydraulic jump; (ii) the specific discharge of the flow that is the discharge per metre of flow width; (iii) the sediment concentration in the flow. Here the model uses: (i) eight possible pre-jump Fr' (1.1 to 6.0); (ii) 20 different discharges (1 to 400 m²/s); and (iii) four

different sediment concentrations (0.5 to 2.0%_{vol}). Together these variables combine into 640 different flows. All of these different flows are fed into the model.

Step 3: Run the model for all specified flow conditions

For all 640 different flows the matching sediment wave geometries are calculated, although some combinations drop out because they do not generate a stable sediment wave geometry. Finally, all of the calculated sediment wave geometries are plotted in a single graph. The graph plots the wavelength on the horizontal axes and the wave height on the vertical axes. The sediment waves are fully determined by these two parameters as the gradients of the stoss side and the lee side are fixed at the gradients measured on the selected sea-floor sediment wave.

Step 4: Select the calculated sediment wave that matches the sea-floor sediment wave

The observed sediment wave height and length is now also plotted in the same graph as the calculated results. Here four options are possible: (i) the sea-floor sediment wave matches the calculated geometry of several calculations, in which case the average flow properties are taken as the outcome; (ii) the sea-floor sediment wave closely matches a single calculation, in which case this simulation is selected as the outcome; (iii) the sea floor sediment wave does not match any calculated sediment wave, but plots closely to a calculated sediment wave, in which case that closely matching the simulation is selected; or (iv) the sea-floor sediment wave does not match any of the calculations, in which case the outcome is that the sediment wave is unlikely to be formed by a cyclic step process.

Working of the model

The model starts its calculation from just upstream of the hydraulic jump at the user specified discharged (Q), densimetric Froude number (Fr') and sediment concentration (C). From here the cyclic step process is broken up into three parts.

Part 1: The hydraulic jump

In this first part of the model the pre-jump Fr'₁ is matched to its conjugate post-jump Fr'₂ using a momentum balance:

$$Fr'_{2} = \frac{2^{3/2}Fr'_{1}}{\left(\sqrt{(1+8Fr'_{1})}-1\right)^{3/2}}$$
 (A1)

The model then uses the definition of the Fr' and Q to calculate the flow depth and flow velocity just downstream of the hydraulic jump:

$$Fr' = \frac{U}{\sqrt{\frac{(\rho_t - \rho_a)}{\rho_t}gH}} \tag{A2}$$

$$Q = UH \tag{A3}$$

Finally the length of the hydraulic jump is calculated using the experimental expression of (Rajaratnam, 1967):

$$L_{iumn} = 4.9 (H_1 - H_2) + 6.1 H_2 \tag{A4}$$

Part 2: The stoss side

Here the boundary conditions (U_2, H_2) are fed in from step 1 to then solve the gradually varying flow equations:

$$\frac{dH}{dx} = \frac{S - f/_8 Fr'}{1 - Fr'} \tag{A5}$$

$$\frac{dU}{dx} = \frac{-U}{H} \frac{dH}{dx} \tag{A6}$$

Before solving these equations, the gradient (S) is set to the gradient of the stoss side of the sea-floor sediment wave. The friction factor (f) is determined iteratively by Colebrook et al., (1939):

$$\frac{1}{f^{1/2}} = -2\log\left(\frac{k_s/_H}{3.7} + \frac{2.51}{Re\,f^{1/2}}\right) \tag{A7}$$

Here the roughness of the sea floor (ks) is set to 2.5 times the grain size (d), and the Reynolds number (Re) is defined as:

$$Re = \frac{HU}{v} \tag{A8}$$

For subcritical flow (Fr' < 1) and a very small or reverse slope (S) the gradually varying flow equations suggest acceleration of the flow ($\frac{dH}{dx}$ < 0) and therefore an increase in the Fr' downstream of the hydraulic jump. The model calculates how long the stoss side needs to be to accelerate the flow to a value of Fr' just below 1.

Part 3: The lee side

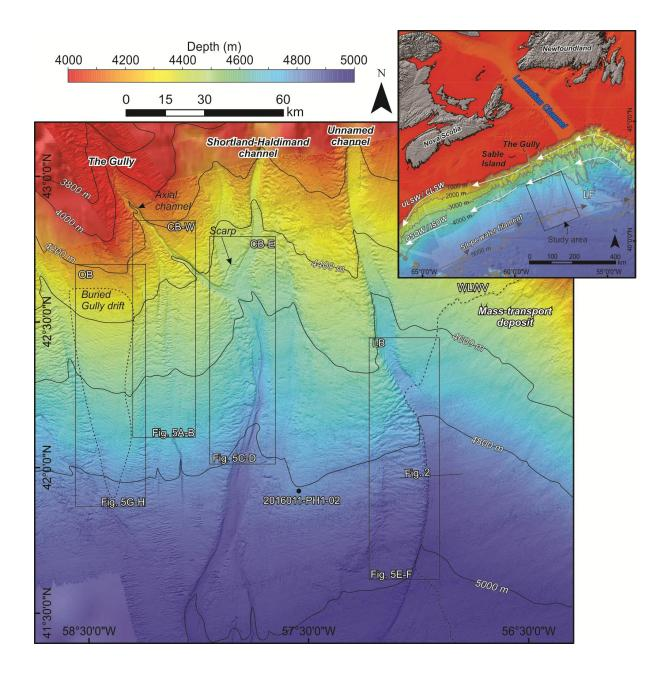
This step repeats the stoss side calculation, but now starts at a value of Fr' just above 1 at the crest and calculates how long a lee side is needed to reach the supercritical pre-jump Fr' again. The gradient is now positive, but given that Fr' > 1 the denominator of Eq. A5 is now negative. This ensures that $\frac{dH}{dx} < 0$ and that the flow will further accelerate.

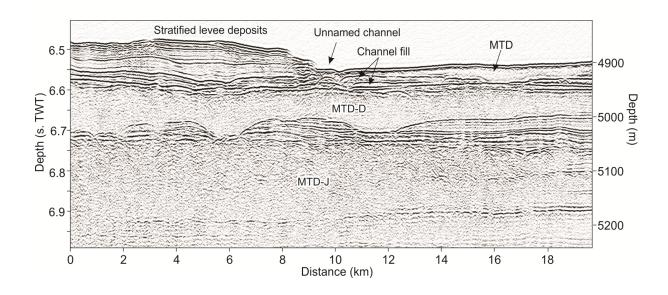
Calculate the sediment wave height and length

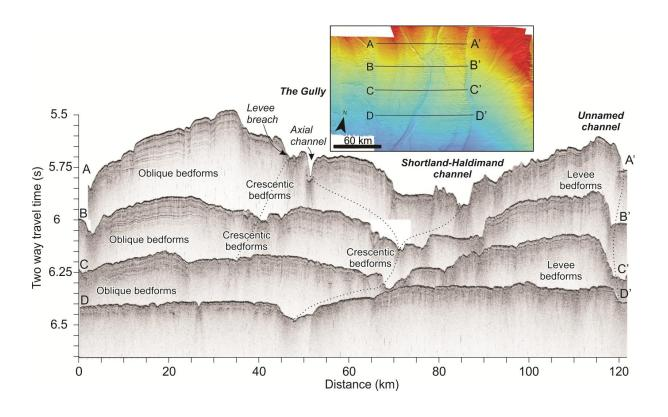
Finally, all results are combined and the overall height and length of the sediment wave are calculated and stored. Then the computation re-starts for the next combination of flow properties.

References

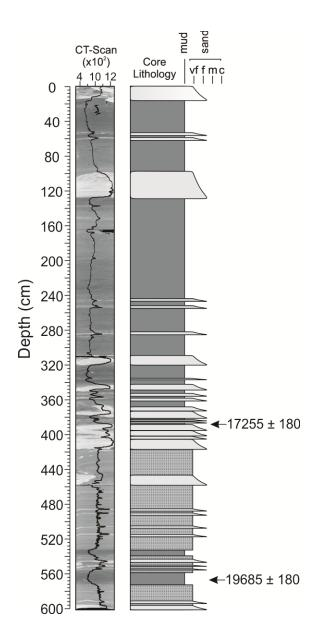
- Cartigny M.J.B., Postma G., van den Berg J.H., and Mastbergen D.R. (2011) A comparative study of sediment waves and cyclic steps based on geometries, internal structures and numerical modeling. *Marine Geology*, **280**, 40–56, doi: 10.1016/j.margeo.2010.11.006.
- Colebrook C.F., Blench T., Chatley H., Essex E.H., Finniecome J.R., Lacey G., Williamson J., and Macdonald G.G. (1939) Turbulent flow in pipes, with particular reference to the transition region between the smooth and the rough piper laws. *Journal of the Institution of Civil engineers*, 12, 393–422.
- **Mastbergen D. R.** and **Van Den Berg J. H.** (2003). Breaching in fine sands and the generation of sustained turbidity currents in submarine canyons. *Sedimentology*, **50**, 625-637.
- **Rajaratnam N.** (1967) Hydraulic jumps, *in* Advances in hydroscience, Elsevier, v. 4, p. 197–280.

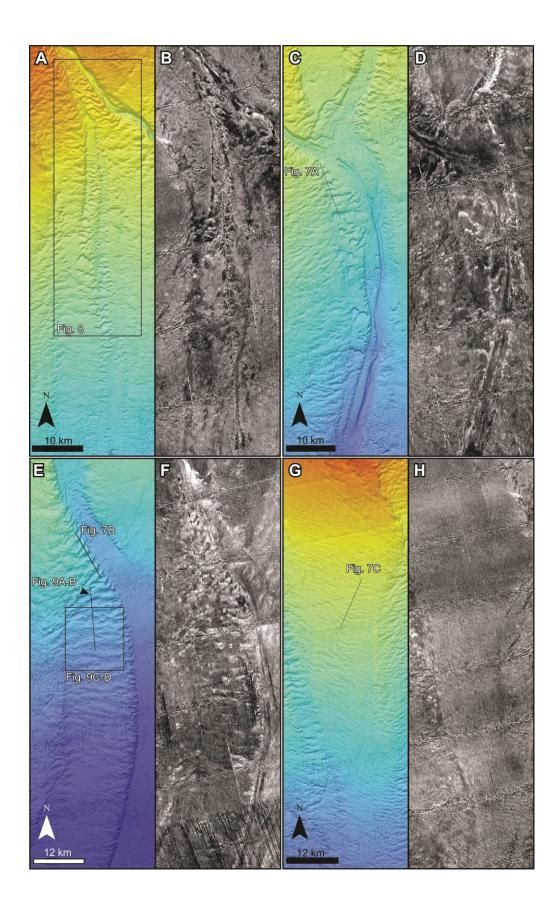


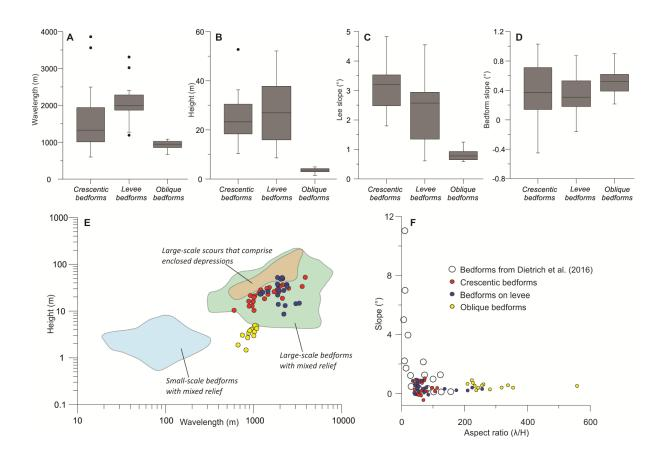


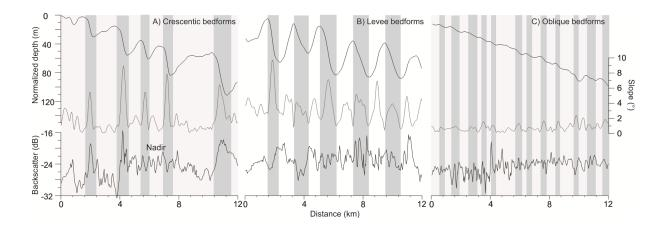


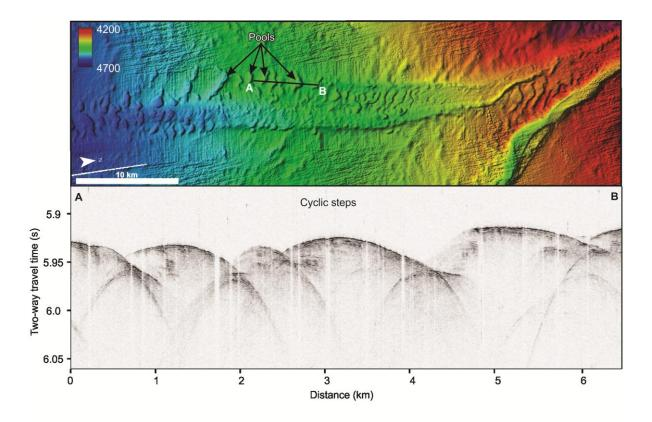
This article is protected by copyright. All rights reserved.

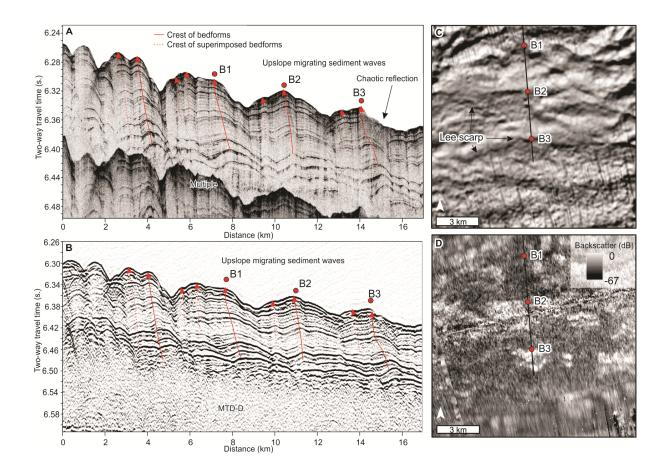


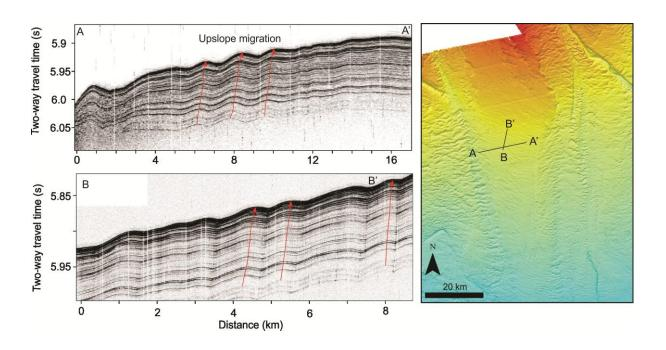












This article is protected by copyright. All rights reserved.

